EXIT Chart-Aided Adaptive Coding for Multilevel BICM With Turbo Equalization in Frequency-Selective MIMO Channels

Shinsuke Ibi, *Member, IEEE*, Tad Matsumoto, *Senior Member, IEEE*, Reiner Thomä, *Fellow, IEEE*, Seiichi Sampei, *Fellow, IEEE*, and Norihiko Morinaga, *Fellow, IEEE*

***Abstract*—This paper proposes an adaptive coding (AC) scheme for multilevel bit-interleaved coded modulation (ML-BICM) with minimum mean-square error (MMSE) turbo equalization in frequency-selective multiple-input–multiple-output (MIMO) channels. The aim of this paper is to minimize the information rate loss due to the mismatch between channel realization and channel coding. With the aid of the knowledge about extrinsic information transfer characteristics at the receiver, code parameters such as code rates and/or generator polynomials are adaptively selected independently for each ML-BICM layer. Model-based simulation results show that an achievable average throughput can be significantly improved with the proposed AC technique over automatic repeat request with fixed coding rate. Furthermore, the advantageous points of the proposed scheme are verified through field-measurement-data-based simulations.**

***Index Terms*—Adaptive coding (AC), bit-interleaved coded modulation (BICM), measurement-data-based simulation, multilevel coding, multiple-input–multiple-output (MIMO), turbo equalization.**

I. Introduction

MINIMUM mean-square error (MMSE) turbo equalization has been recognized as one of the most promising techniques in broadband mobile communication applications using single-carrier signaling [1]–[4]. To improve the band efficiency of broadband single-carrier systems, Dejonghe and Vandendorpe [5] apply the MMSE turbo equalization technique to bit-interleaved coded modulation (BICM) [6] using higher-order modulation such as quadrature amplitude modulation (QAM) constructed with arbitrary mapping rules. The technique presented in [7] restricts the mapping rule in such a way that the QAM constellation is constructed by linearly weighed multiple binary sequences, by which the equalizer can separate the transmitted binary sequences constituting the QAM constellation. This technique is referred to as multilevel (ML)-BICM with turbo equalization, where the terminology "level" corresponds to each of the binary sequences. In fact, the ML-BICM approach can achieve a much higher throughput efficiency over BICM when applied to automatic repeat request (ARQ), where, to best exploit the cross-level separability, retransmission control independently takes place level by level. Despite the throughput merit achieved by ML-BICM with the level-wise ARQ technique, there still remains an equalizer-code mismatch between the given channel realization and the coding scheme used for each level, which results in two detrimental situations: 1) The code redundancy is too high to maintain the information rate inherently bearable by the channel itself; and 2) the turbo equalization does not converge. This implicitly means that if the code parameters are adaptively selected at each level in ML-BICM turbo equalization, further throughput improvement can be provisioned. This technique is referred to as ML-BICM with adaptive coding (ML-BICM AC) [8]. This paper provides a more in-depth analysis for ML-BICM AC than that described in [8] and introduces another code selection criterion to achieve better performance.

Recently, multiple-input–multiple-output (MIMO) radio network configurations have been recognized as being able to drastically improve the spectrum efficiency of wireless communication systems. MIMO systems assume the use of multiple antennas at both the transmitter (Tx) and receiver (Rx) sides. Extension of the MMSE turbo equalization to MIMO is straight forward. Interference due to spatial multiplexing can be canceled in the same way as intersymbol interference is suppressed by the soft cancellation and MMSE filtering in the MMSE turbo equalizer [9]. It is well known that the convergence properties of turbo Rxs using multiple antennas, in general, deeply depend on the propagation channels' spatiotemporal structure [10]: This motivates the idea that ML-BICM AC should be combined with multi-antenna transmission in MIMO, where the code parameters are adaptively controlled not only on antenna-by-antenna but also on level-by-level bases, depending on the channel's temporal and spatio characteristics.

The primary focus of this paper is on ML-BICM AC with MMSE turbo equalization in frequency-selective MIMO

Manuscript received February 8, 2006; revised January 22, 2007 and April 8, 2007. The review of this paper was coordinated by Dr. M. Valenti.

S. Ibi and S. Sampei are with the Graduate School of Engineering, Osaka University, Osaka 565-0871, Japan (e-mail: ibi@comm.eng.osaka-u.ac.jp; sampei@comm.eng.osaka-u.ac.jp).

T. Matsumoto is with the Centre for Wireless Communications, University of Oulu, 90570 Oulu, Finland, and also with the Japan Advanced Institute of Science and Technology, Ishikawa 923-1292, Japan (e-mail: tadashi.matsumoto@ee.oulu.fi).

R. Thomä is with the Electronic Measurement Research Laboratory, Ilmenau University of Technology, 98684 Ilmenau, Germany (e-mail: Reiner.Thomae@TU-Ilmenau.de).

N. Morinaga is with the Department of Information Technology, Hiroshima International University, Hiroshima 737-0112, Japan (e-mail: morinaga@it.hirokoku-u.ac.jp).

Color versions of one or more of the figures in this paper are available online at http://ieeexplore.ieee.org.

Digital Object Identifier 10.1109/TVT.2007.901959

channels, where the aim is to minimize the information rate loss due to the mismatch between channel realization and channel coding. With the aid of the knowledge about extrinsic information transfer (EXIT) characteristics [11], code parameters such as code rates and/or generator polynomials should be adaptively selected independently for each QAM level so that the information rate loss is minimized. The information about the selected code set is then fed back to the Tx via a feedback channel, and the selected codes are used for the next transmission, where it is assumed that the channels are constant over at least two consecutive transmission frames.

This paper then zeros in on the use of multidimensional channel-sounding field measurement data in offline simulations to verify the advantageous points of the proposed AC scheme in real fields. A measurement campaign took place in a courtyard in the campus of Ilmenau University of Technology, Ilmenau, Germany. The sequence of channel impulse response (CIR) from each of the Tx multiple antenna elements to each of the Rx antenna elements was measured [12], and the results are used in offline simulations. Furthermore, the outcomes of the measurement-data-based simulations are correlated with the results of channel analysis performed to identify the MIMO channel's spatial characteristics, such as direction-of-departure and direction-of-arrival [13]–[15]. The objective of the measurement-data-based simulations in this paper is to better understand the performance tendencies of the proposed MIMO ML-BICM AC technique in various channel characteristics in real fields.

The major contributions of this paper are summarized as follows: Section II introduces the channel and system models used in this paper for MMSE turbo equalization. This paper uses a frequency-domain version [3], [16], [17] of the ML-BICM MMSE turbo equalization because of its low complexity. The equalization algorithm is adequately modified to be suited for the AC scheme without making any significant approximations in the technique. Section III derives the proposed AC scheme that adaptively selects the codes considered most suitable, given the channel's characteristics, from among the predetermined code set. The scheme is explained in the context of examining the equalizer's convergence property through EXIT chart analysis demonstrating the two detrimental situations. Practical issues related to the proposed AC scheme are also discussed in Section III. Section IV presents the results of simulations conducted to evaluate the throughput efficiency achieved by the ML-BICM AC. In Section V, the performance of the proposed technique is further evaluated in real fields using field measurement data, and the performance tendencies are correlated with the spatial channel properties for better understanding of the behavior of the proposed scheme in various channel characteristics.

II. System Model

A. Signal Model

1) Channel Model: Let us assume that the system employs M Tx and N Rx antennas. The symbols to be transmitted are spatially multiplexed and sent from the multiple Tx antennas, where the complex baseband signal to be transmitted from the mth Tx antenna at the discrete kth symbol timing is denoted by $s_m(k)$. Let the CIR between the mth Tx and nth Rx antennas, which is superimposed with the Tx and Rx filters, be denoted by $h_{nm}(t = lT_s) = h_{nm}(l)$, where T_s is the symbol duration. The received symbol $r_n(k)$, which is received by the nth Rx antenna, is then in the discrete-time domain given by

$$r_n(k) = \sum_{l=0}^{L-1} \sum_{m=1}^{M} h_{n,m}(l) s_m(k-l) + \nu_n(k) \tag{1}$$

where L denotes the channel memory length of the CIR, and $\nu_n(k)$ represents the zero-mean additive white Gaussian noise with variance σ_ν^2, for which a circular power distribution in the complex equivalent baseband domain is assumed. For a straightforward application of the frequency-domain filtering technique at the Rx, we assume a length P-symbol cyclic prefix (CP) to be appended to the head of the block comprised of K-coded symbols, which results in $P + K$ symbols in the frames transmitted from each of the m transmit antennas. Making the best use of the CP transmission, it is well known that the channel can be expressed by a block circular matrix whose derivation is summarized in the following: After the space–time sampling of the received signal and removing CP at the Rx, (1) reduces to a vector notation as

$$\boldsymbol{r} = \boldsymbol{H}\boldsymbol{s} + \boldsymbol{\nu} \tag{2}$$

where $\boldsymbol{r}$, $\boldsymbol{s}$, and $\boldsymbol{\nu}$ are the received signal, transmitted signal, and Gaussian noise vectors, respectively, given by

$$\boldsymbol{r} = \left[\boldsymbol{r}_1^T, \ldots, \boldsymbol{r}_n^T, \ldots, \boldsymbol{r}_N^T\right]^T \tag{3}$$

$$\boldsymbol{s} = \left[\boldsymbol{s}_1^T, \ldots, \boldsymbol{s}_m^T, \ldots, \boldsymbol{s}_M^T\right]^T \tag{4}$$

$$\boldsymbol{\nu} = \left[\boldsymbol{\nu}_1^T, \ldots, \boldsymbol{\nu}_n^T, \ldots, \boldsymbol{\nu}_N^T\right]^T \tag{5}$$

and their component vectors are

$$\boldsymbol{r}_n = [r_n(1), \ldots, r_n(k), \ldots, r_n(K)]^T \tag{6}$$

$$\boldsymbol{s}_m = [s_m(1), \ldots, s_m(k), \ldots, s_m(K)]^T \tag{7}$$

$$\boldsymbol{\nu}_n = [\nu_n(1), \ldots, \nu_n(k), \ldots, \nu_n(K)]^T. \tag{8}$$

The block circular channel matrix is then defined as

$$\boldsymbol{H} = [\boldsymbol{H}_1, \ldots, \boldsymbol{H}_m, \ldots, \boldsymbol{H}_M] \tag{9}$$

where its submatrix is

$$\boldsymbol{H}_m = \left[\boldsymbol{H}_{1,m}^T, \ldots, \boldsymbol{H}_{n,m}^T, \ldots, \boldsymbol{H}_{N,m}^T\right]^T \tag{10}$$

and $\boldsymbol{H}_{n,m}$ is a circular matrix based on the column vector $[h_{n,m}(0), \ldots, h_{n,m}(L-1), \boldsymbol{0}_{K-L}]^T$. Note that $\boldsymbol{0}_x$ denotes an all-zero vector with length x.

2) ML-BICM Signaling: The signal vector $\boldsymbol{s}_m$ to be sent from the mth Tx antenna is constructed from independent binary-coded sequences that are linearly weighted and summed up to construct 2^Q QAM constellation points, according to the ML-BICM mapping rule described in [7]. Note that Q denotes

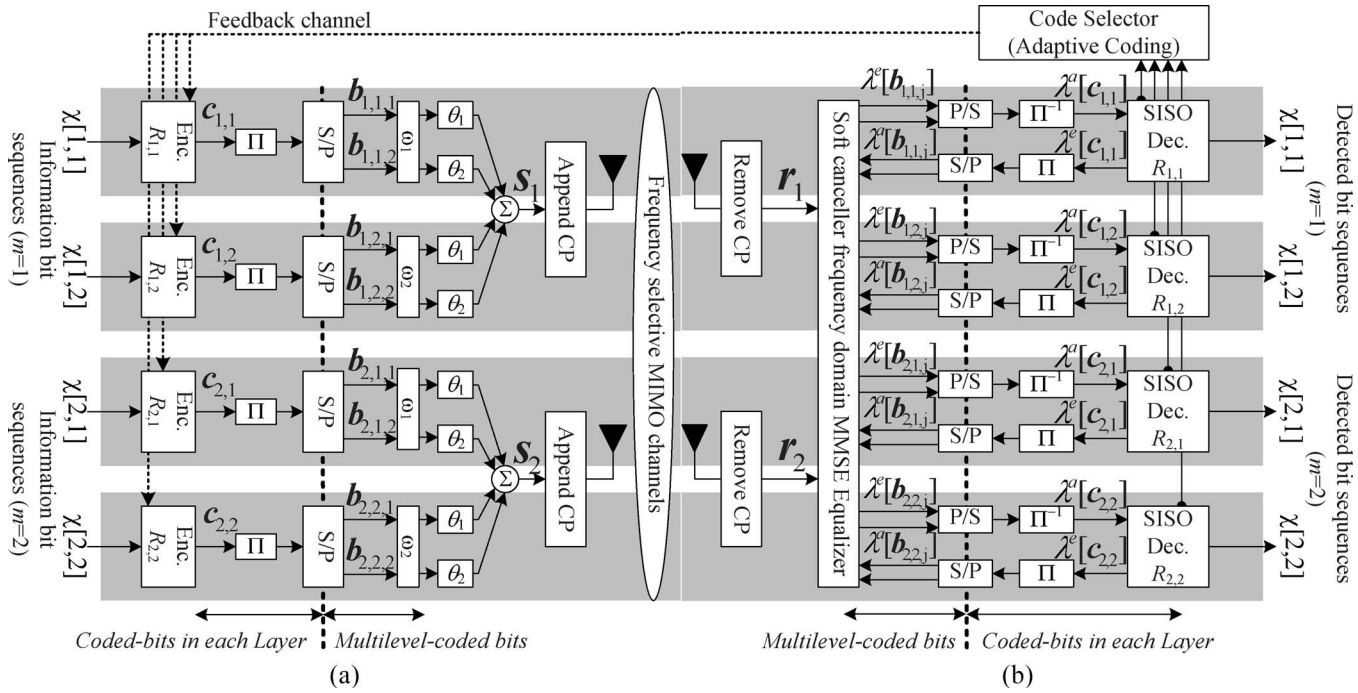

Fig. 1. (a) Block diagram of the Tx: $M = 2$, and $Q = 4$ (16-QAM). (b) Block diagram of the turbo Rx: $N = 2$, and $Q = 4$ (16-QAM).

the number of bits per symbol. A block diagram of the Tx considered in this paper is shown in Fig. 1(a). There are $MQ/2$ layers denoted as $\chi[m, q]$ $(m = 1, \ldots, M,\ q = 1, \ldots, Q/2)$ with the M Tx antennas since the 2^Q QAM signal consists of $Q/2$ layers. Note that the terminology "layer" corresponds to the quaternary phase-shift-keying sequence constituting the QAM constellation and as noted before "level" to the binary sequence. An independent information bit sequence loaded into the layer $\chi[m, q]$ is encoded by its encoder selected from among the available code sets at the Rx, where the Tx is notified of the code selected for each layer via the feedback channel.

Now, we define the following block-wise-coded bit vector to be transmitted over the layer $\chi[m, q]$:

$$\boldsymbol{c}_{m,q} = [c_{m,q}(1), \ldots, c_{m,q}(k'), \ldots, c_{m,q}(2K)]^T \tag{11}$$

where k' denotes the bit index after encoding. Note that since each layer transmits 2 bits per symbol via the in-phase and quadrature channels, which are referred to as I- and Q-channels, respectively, for convenience, the length of the encoded bit vector is $2K$. $c_{m,q}(k') \in \{\pm 1\}$ is a coded bit after encoding. Each layer's coded bit sequence $\boldsymbol{c}_{m,q}$ having $2K$ bits is then interleaved and serial-to-parallel (S/P) converted into two multilevel-coded bit sequences having K bits to be transmitted over the I- and Q-channels of the corresponding layer. Now, we define the following block-wise multilevel-coded bit vector as

$$\boldsymbol{b}_{m,q,j} = [b_{m,q,j}(1), \ldots, b_{m,q,j}(k), \ldots, b_{m,q,j}(K)]^T \tag{12}$$

where k denotes the bit index after S/P conversion, and $b_{m,q,j}(k) \in \{\pm 1\}$ is, with $j = 1$ and 2 corresponding to the I- and Q-channels, respectively, a multilevel-coded bit after S/P conversion. The multilevel-coded bit sequences to be sent over the mth Tx antenna are then linearly weighted and summed up to construct 2^Q QAM constellation points. Thus, the transmitted signal vector $\boldsymbol{s}_m$ is expressed as

$$\boldsymbol{s}_m = \sum_{q=1}^{Q/2} \omega_q \sum_{j=1}^{2} \theta_j \boldsymbol{b}_{m,q,j} \tag{13}$$

where the mapping coefficients are defined as

$$\theta_1 = 1, \quad \theta_2 = \sqrt{-1} \tag{14}$$

$$[\omega_1, \ldots, \omega_{Q/2}] = \begin{cases} [1], & /\sqrt{2}\ (Q=2) \\ [2 \quad 1], & /\sqrt{10}\ (Q=4) \\ [4 \quad 2 \quad 1], & /\sqrt{42}\ (Q=6). \end{cases} \tag{15}$$

B. MMSE Turbo Rx

1) Iterative Decoding: Fig. 1(b) shows a block diagram of the space–time turbo Rx for MIMO ML-BICM signaling. The turbo Rx is comprised of a soft-canceling MMSE equalizer and soft-input–soft-output (SISO) decoders [18]. The equalizer produces an *extrinsic* log-likelihood ratio (LLR) for each multilevel-coded bit $b_{m,q,j}(k)$ as

$$\lambda^e\left[b_{m,q,j}(k)\right] = \ln \frac{\text{Prob.}\left[z_m(k) | b_{m,q,j}(k) = +1\right]}{\text{Prob.}\left[z_m(k) | b_{m,q,j}(k) = -1\right]} \tag{16}$$

where $z_m(k)$ denotes the MMSE equalizer output defined later in (29). More details about the derivation of (16) will be explained later in the context of deriving (31). $\lambda^e[b_{m,q,1}(k)]$ and $\lambda^e[b_{m,q,2}(k)]$ are the LLRs of the bits transmitted via the I- and Q-channels, respectively, of the corresponding layer $\chi[m, q]$. The output bit-wise LLRs are parallel-to-serial (P/S) converted and deinterleaved to yield the LLR sequence of the layer

$\chi[m,q]$'s coded bits having length of $2K$, which is denoted as $\lambda^a[c_{m,q}(k')]$, and it is then delivered to the SISO decoder as *a priori* LLR.

Maximum *a posteriori* probability (MAP) SISO decoding of the channel code derives the *extrinsic* LLR $\lambda^e[c_{m,q}(k')]$ as

$$\lambda^e\left[c_{m,q}(k')\right] = \lambda^p\left[c_{m,q}(k')\right] - \lambda^a\left[c_{m,q}(k')\right] \tag{17}$$

where the *a posteriori* LLR $\lambda^p[c_{m,q}(k')]$ is directly calculated with the MAP algorithm by utilizing the knowledge about the code's redundancy (or trellis) structure, i.e.,

$$\lambda^p\left[c_{m,q}(k')\right] = \ln \frac{\text{Prob.}\left[c_{m,q}(k') = +1 | \lambda^a[\boldsymbol{c}_{m,q}]\right]}{\text{Prob.}\left[c_{m,q}(k') = -1 | \lambda^a[\boldsymbol{c}_{m,q}]\right]}. \tag{18}$$

The *extrinsic* LLRs associated with each layer's coded bits $\lambda^e[c_{m,q}(k')]$ are then interleaved and S/P converted into two LLR streams to be fed back to the equalizer, which defines the equalizer's *a priori* LLR $\lambda^a[b_{m,q,j}(k)]$. The key point of iterative decoding is that the *extrinsic* LLRs are propagated and exchanged several times between the equalizer and the decoder. It is well known that the *extrinsic* LLR monotonically increases as the *a priori* LLR increases.

2) Soft Canceling MMSE Equalization: For the soft cancellation of interference components, a soft-replica vector $\boldsymbol{H}\hat{\boldsymbol{s}}$, whose elements are the replicated symbol of the interference components, is subtracted from the received signal $\boldsymbol{r}$ as

$$\tilde{\boldsymbol{r}} = \boldsymbol{r} - \boldsymbol{H}\hat{\boldsymbol{s}} \tag{19}$$

where the vector $\tilde{\boldsymbol{r}}$ is referred to as the interference residual, with $\hat{\boldsymbol{s}}$ and $\hat{\boldsymbol{s}}_m$, respectively, being

$$\hat{\boldsymbol{s}} = \left[\hat{\boldsymbol{s}}_1^T, \ldots, \hat{\boldsymbol{s}}_m^T, \ldots, \hat{\boldsymbol{s}}_M^T\right]^T \tag{20}$$

$$\hat{\boldsymbol{s}}_m = \left[\hat{s}_m(1), \ldots, \hat{s}_m(k), \ldots, \hat{s}_m(K)\right]^T. \tag{21}$$

$\hat{s}_m(k)$ is an expected symbol conditioned upon the decoder feedback given by

$$\begin{aligned}\hat{s}_m(k) &= \mathbb{E}\left\{s_m(k)\right\} \\ &= \sum_{s_i^c \in \mathcal{S}} s_i^c \text{Prob.}\left[s_m(k) = s_i^c\right]\end{aligned} \tag{22}$$

where $\mathbb{E}\{\cdot\}$ denotes the expectation, Prob.$[s_m(k) = s_i^c]$ is the symbol's *a priori* probability, and each s_i^c is the symbol in the constellation set $\mathcal{S}$. Assuming that the feedback consists of independent bit likelihoods, the symbol *a priori* probability can be computed by the product of the bit-wise *a priori* probabilities as [19]

$$\Pr\left[s_m(k) = s_i^c\right] = \prod_{q=1}^{Q/2} \prod_{j=1}^{2} \Pr\left[b_{m,q,j}(k) = b_{q,j}^c\right] \tag{23}$$

where $s_i^c = \sum_{q=1}^{Q/2} \omega_q \sum_{j=1}^{2} \theta_j b_{q,j}^c$ is formed by the bit candidates $b_{q,j}^c \in \{\pm 1\}$, and the bit-wise *a priori* probability is given by

$$\Pr\left[b_{m,q,j}(k) = b_{q,j}^c\right] = \frac{1}{2}\left[1 + b_{q,j}^c \tanh\left[\frac{\lambda^a\left[b_{m,q,j}(k)\right]}{2}\right]\right]. \tag{24}$$

In the case of ML-BICM, due to the independency between the I- and Q-channels, a small effort in algebraic manipulation reduces (22) to

$$\hat{s}_m(k) = \sum_{q=1}^{Q/2} \omega_q \sum_{j=1}^{2} \theta_j \tanh\left[\frac{\lambda^a\left[b_{m,q,j}(k)\right]}{2}\right]. \tag{25}$$

Next, an adaptive linear filter is used to extract the desired signal components s_m as follows: The matrix $\boldsymbol{W}_m$ of the filter taps is optimized to minimize the following mean-square error (MSE):

$$\text{MSE} = \mathbb{E}\left\{\left|\boldsymbol{W}_m^H\left[\tilde{\boldsymbol{r}} + \boldsymbol{H}_m\hat{\boldsymbol{s}}_m\right] - \boldsymbol{s}_m\right|^2\right\} \tag{26}$$

where the output vector $\boldsymbol{z}_m$ is given by

$$\boldsymbol{z}_m = \boldsymbol{W}_m[\tilde{\boldsymbol{r}} + \boldsymbol{H}_m\hat{\boldsymbol{s}}_m] \tag{27}$$

with

$$\boldsymbol{z}_m = \left[z_m(1), \ldots, z_m(k), \ldots, z_m(K)\right]^T. \tag{28}$$

The filter output $\boldsymbol{z}_m$ can be efficiently derived by frequency-domain processing [3], [17], which is given in the Appendix for the sake of completeness of this paper.

To calculate the equalizer output *extrinsic* LLR, it is assumed that $z_m(k)$ can be approximated as an output of a Gaussian channel defined by

$$z_m(k) = \mu_m s_m(k) + \psi_m(k) \tag{29}$$

where $\psi_m(k)$ represents a zero-mean independent complex Gaussian noise with variance σ_m^2. Note that μ_m and σ_m^2 are calculated along with the MMSE filtering process, as described in the Appendix. Using the Gaussian approximation of (29), the probability density function (pdf) $p_{\mathcal{Z}|\mathcal{S}}(z_m(k)|s_i^c)$ of $z_m(k)$ conditioned upon the symbol constellation set is given by

$$p_{\mathcal{Z}|\mathcal{S}}\left(z_m(k)|s_i^c\right) = \frac{1}{\pi\sigma_m^2} \exp\left(-\frac{|z_m(k) - \mu_m s_i^c|^2}{\sigma_m^2}\right). \tag{30}$$

Thus, the *extrinsic* LLR $\lambda^e[b_{m,q,j}(k)]$ of the layer $\chi[m,q]$'s coded bit can be computed by using the *a priori* probability of (24) as[1] [19], [20] that in (31), shown at the bottom of the next page.

[1]The LLR derivation can further be simplified, as shown in [7], by invoking an assumption of independency among the bit LLRs in the constellation, regardless of the modulation format used in ML-BICM signaling. This is true only if the *a priori* information feedback from the SISO decoders is perfect. Otherwise, the independency does not hold due to the imperfect interference cancellation. For the sake of accuracy in LLR computation, this paper uses the exact formula given in (31).

III. EXIT-AIDED AC

A. EXIT Properties for ML-BICM

The mutual information (MI) $\mathcal{I}$ between the coded bits $\mathcal{C} \in \{\pm 1\}$ and the LLR λ is, if the occurrencesof $\mathcal{C} = -1$ and $+1$ are equiprobable, given by [11]

$$\begin{aligned}\mathcal{I} &= \frac{1}{2}\sum_{\mathcal{C}\in\pm 1}\int_{-\infty}^{\infty} p_{\lambda|c}(\xi|\mathcal{C}) \\ &\quad \cdot \log_2\left(\frac{2p_{\lambda|c}(\xi|\mathcal{C})}{p_{\lambda|c}(\xi|-1)+p_{\lambda|c}(\xi|+1)}\right)d\xi \\ &= 1 - \int_{-\infty}^{\infty} p_{\lambda|c}(\xi|+1)\log_2\left(1+e^{-\xi}\right)d\xi \end{aligned} \tag{32}$$

where $p_{\lambda|c}(\xi|\mathcal{C}) = \text{Prob.}[\lambda = \xi | c = \mathcal{C}]$ is the pdf of the LLR being ξ conditioned upon the coded bit $\mathcal{C}$. Note that the last line in (32) has been derived based on the consistency condition on the LLR pdf [21], where account is taken of the symmetric property in its shape, as

$$p_{\lambda|c}(\xi|+1) = e^{\xi} p_{\lambda|c}(\xi|-1). \tag{33}$$

Thus, the MI for the equalizer and decoder outputs $I^{\mathrm{E}}_{m,q}$ and $I^{\mathrm{D}}_{m,q}$, respectively, can be calculated by evaluating (32), for which however the pdf $p_{\lambda|c}(\xi|\mathcal{C}) = \text{Prob.}[\lambda = \xi | c = \mathcal{C}]$ has to be obtained. An easy way to obtain the pdf is to measure the histogram of the LLRs $\lambda^a[c_{m,q}(k')]$ and $\lambda^e[c_{m,q}(k')]$ through simulations.

Despite the ease in calculating the MI of the equalizer output, analyzing the EXIT characteristic of each layer is not easy because a certain layer's MI transfer depends on other layers', which is formulated by

$$\begin{aligned} I^{\mathrm{E}}_{m,q} = F_{m,q}\Big(&I^{\mathrm{D}}_{1,1},\ldots,I^{\mathrm{D}}_{1,Q/2},\ldots,I^{\mathrm{D}}_{m,1} \\ &\ldots,I^{\mathrm{D}}_{m,Q/2},\ldots,I^{\mathrm{D}}_{M,1},\ldots,I^{\mathrm{D}}_{M,Q/2}\Big). \end{aligned} \tag{34}$$

This fact results in the difficulty in visualizing how effectively the MI transfer from a certain layer has helped the other layers' convergence when the number of layers is larger than 1. An example of the 2-D EXIT surfaces for a two-layered BICM equalizer is depicted in Fig. 2, where $M = 1$, $N = 2$, $Q = 4$ (16-QAM), 24-path frequency-selective fading with an exponential decay factor of 2 dB, and the symbol energy-to-noise density ratio of $E_s/N_0 = 8$ dB per receive antenna were assumed. Note that the definition of E_s/N_0 is per receive antenna throughout in this paper. The coded frame length of $2K$ was assumed to be 4096, and to ensure the accuracy of the pdf evaluation for the MI calculation, ten frames were transmitted for the LLR histogram measurement to draw the 2-D EXIT chart. The result is shown in Fig. 3. In this 2-D case, the EXIT characteristic is expressed by *planes* since each MI depends on the feedback MI from both decoders of the two layers as

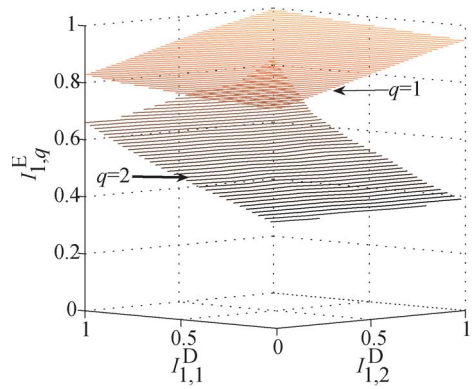

Fig. 2. EXIT surfaces of the equalizer. Example snapshot of $L = 24$ and instantaneous $E_s/N_0 = 8$ dB per receive antenna.

$$I^{\mathrm{E}}_{1,q} = F_{1,q}\left(I^{\mathrm{D}}_{1,1}, I^{\mathrm{D}}_{1,2}\right), \quad (q = 1, 2). \tag{35}$$

An important observation of Fig. 2 is that the EXIT *planes* corresponding to layers $\chi[1,1]$ and $\chi[1,2]$ are separated with each other because of ML-BICM, which is constructed by linearly combining the weighted coded sequences. The layer separability suggests that different code parameters be independently made controllable layer by layer so that, as a whole, the layer's information-bearing capability can be best exploited. Furthermore, different codes for each layer should be used in different channel realizations since the *planes* are time-varying functions.

Fig. 3(a) shows the EXIT characteristics of several channel decoder MIs for the constraint length 4 convolutional codes specified in [22], as summarized in Table I. The EXIT curves in this figure are for coding rates $\mathcal{R}$ from 1/8 to 7/8, as described in the figure caption. The relationship between the equalizer output MI and each code's frame error rate (FER) is presented in Fig. 3(b). The frame length of $2K$ comprised of coded bits was assumed to be 4096. The decoder MI transfer function is denoted by

$$I^{\mathrm{D}}_{m,q} = G_{\mathcal{R}}\left(I^{\mathrm{E}}_{m,q}\right). \tag{36}$$

Basically, the bit error rate and its corresponding FER can be estimated based on the MI calculated from the decoder's *a posteriori* LLR distribution [11]. In addition, there is a one-to-one mapping between $I^{\mathrm{E}}_{m,q}$ and the decoder's *a posteriori* MI

$$\lambda^e\left[b_{m,q,j}(k)\right] = \ln \frac{\sum_{s_i^c \in \left\{\mathcal{S}|b^c_{q,j}=+1\right\}} \left(p\left(z_m(k)|s_i^c\right)\Pr\left[s_m(k)=s_i^c\right] / \Pr\left[b_{m,q,j}(k)=b^c_{q,j}\right]\right)}{\sum_{s_i^c \in \left\{\mathcal{S}|b^c_{q,j}=-1\right\}} \left(p\left(z_m(k)|s_i^c\right)\Pr\left[s_m(k)=s_i^c\right] / \Pr\left[b_{m,q,j}(k)=b^c_{q,j}\right]\right)} \tag{31}$$

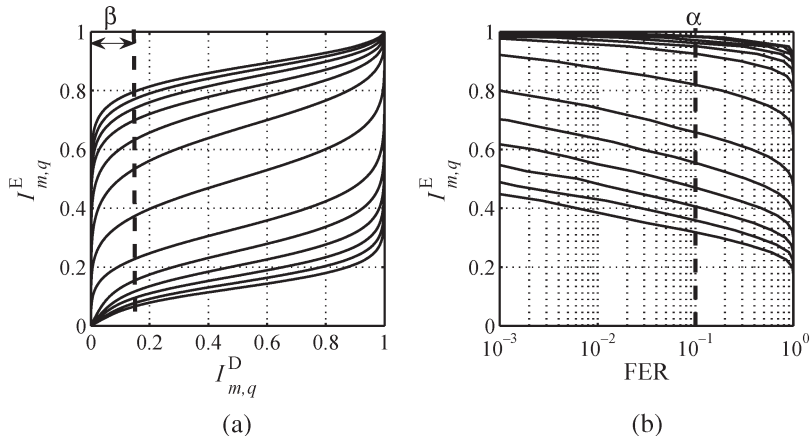

Fig. 3. (a) EXIT characteristics of decoders. (b) FER versus $I^{\mathrm{E}_{m,q}}$. Coding rates $\mathcal{R} = 7/8, 6/7, 5/6, 4/5, 3/4, 2/3, 1/2, 1/3, 1/4, 1/5, 1/6, 1/7,$ and $1/8$ with constraint length 4 from top to bottom.

TABLE I
LIST OF AVAILABLE CODES IN THIS PAPER

Rate ($\mathcal{R}$)	Generators in octal	d_{free}
1/8	17 17 13 13 13 15 15 17	26
1/7	17 17 13 13 13 15 15	23
1/6	17 17 13 13 15 15	20
1/5	17 17 13 15 15	16
1/4	13 15 15 17	13
1/3	13 15 17	10
1/2	15 17	6
2/3	15 17 (11 10)	4
3/4	15 17 (11 10 01)	4
4/5	15 17 (11 01 10 10)	3
5/6	15 17 (11 01 10 01 01)	3
6/7	15 17 (11 01 01 01 10 10)	2
7/8	15 17 (11 01 01 01 01 10 01)	2

( ) denotes Puncturing table

due to the serial-concatenated structure where the decoder input is connected only to the equalizer output LLR.

To assess the code optimality in terms of the convergence property, given the channel realization, the equalizer and decoder MI transfer characteristics are depicted in Fig. 4 for the two detrimental cases introduced in Section I: Fig. 4(a) is for the case where the code redundancy is too high to fully exploit the channel's inherent capability; and Fig. 4(b) is where turbo equalization does not converge. For an $(M, N) = (2, 2)$ MIMO system, the trajectories of MI exchange until the eighth iteration are plotted in the figures for *instantaneous* $E_s/N_0 = 10$ dB. The other simulation parameters are the same as those used in Fig. 2. There are four trajectories corresponding to layers $\chi[1, 1]$, $\chi[1, 2]$, $\chi[2, 1]$, and $\chi[2, 2]$. Note that multidimensional equalizer functions $F_{m,q}$ are depicted by projection so that only the lower and upper bounds are shown. The lower bound is calculated by setting the decoder MI of the other layers at 0 and the upper bound by setting the MI of the other layers at 1. Fig. 4(a) corresponds to the case where a higher $I^{\mathrm{D}}_{m,q}$ can be achieved even at the first iteration. In this case, the role of the MI exchange between the equalizer and the decoder is not significant, which means that an information rate loss due to equalizer-code mismatch is inevitably incurred. This suggests that such a rate loss be reduced by using a higher code rate. In contrast, Fig. 4(b) shows the case where the equalizer and decoder EXIT curves intersect at a point that yields a relatively low decoder *a posteriori* MI, which results in a high FER. It should be noted that the second case happens likely if the feedback MI $I^{\mathrm{D}}_{m,q}$ resulting from the first iteration is not high enough. Such observations lead to the idea that the code parameters be selected to ensure the best matching between the equalizer and the code.

B. AC Using EXIT Chart

To avoid the two detrimental cases demonstrated in Section III-A, the optimal codes for each layer of ML-BICM may be found based on the area property analysis [21]. However, in practice, this is not feasible because of the too-high computational complexity required to find multidimensional equalizer EXIT functions $F_{m,q}$. In addition, the available code parameters are presumably limited. Therefore, adjusting the code parameters in real time such that the code optimality in a strict sense is always guaranteed is not practical. Taking into account these constraints, a practical approach is to use a code considered most reasonable based on the EXIT trajectory plots resulting from the previous frame transmission for each layer,[2] by which the rate loss is reduced while the designed target FER is achieved: The code is selected from among the prepared code set, and the channels are assumed to stay the same over the two consecutive frame timings. Now, we focus on the trajectory in the EXIT chart.

As noted above, the FER after decoding can be estimated from $I^{\mathrm{E}}_{m,q}$ at the terminal point $I^{\mathrm{E(end)}}_{m,q}$ of the trajectory by referring the terminal point equalizer MI to the decoder's EXIT curve shown in Fig. 3(a). Note that the terminal point is either the cross-over point between the equalizer and the decoder curves or the point corresponding to the decoder output MI asymptotically being 1.0 ($I^{\mathrm{D}}_{m,q} \approx 1$). The most important observation is that $I^{\mathrm{E(end)}}_{m,q}$ is independent of the other layers at the point where the trajectory converges, as shown in Fig. 4(a). This is because in such a situation, almost a perfect decoder

[2]Along with the turbo iterations, it is easy to perform online measurement of the trajectory only by using the received signal samples, as explained in Section III. Please see also (42).

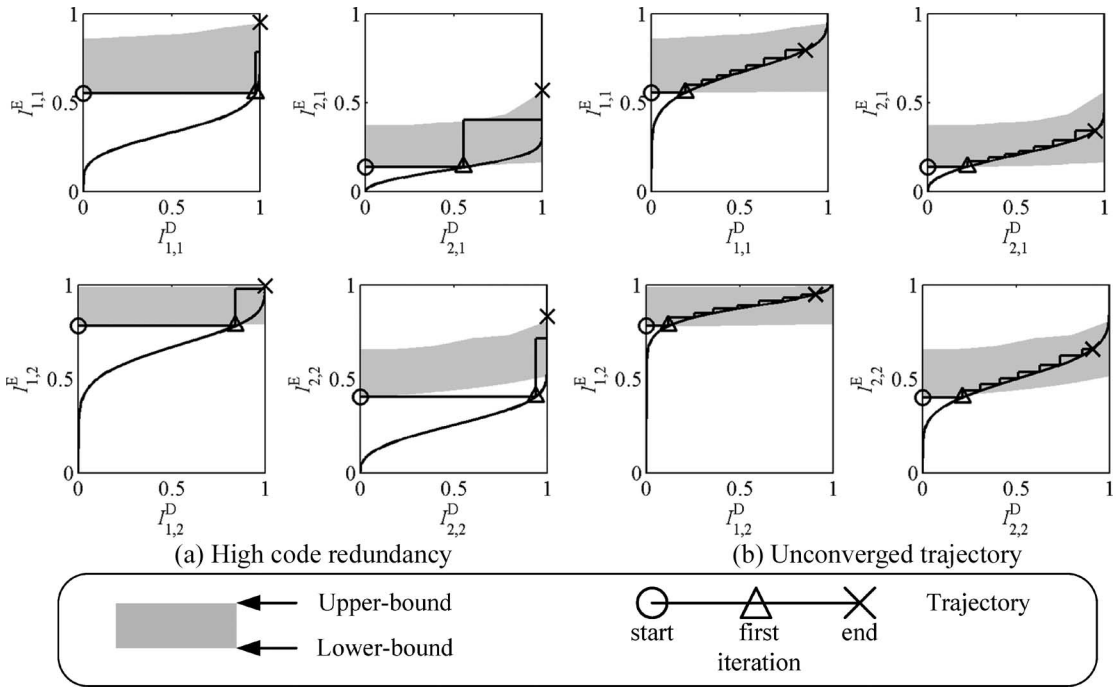

Fig. 4. Snapshots of trajectories in iterative decoding. Code rates (a) $R_{m,q} = 1/3, 1/8, 2/3,$ and $1/4$ and (b) $R_{m,q} = 2/3, 1/5, 7/8,$ and $1/2$ are used for $\chi[1,1]$, $\chi[1,2]$, $\chi[2,1]$, and $\chi[2,2]$, respectively.

a posteriori MI ($I^{\mathrm{D}}_{m,q} \approx 1$) is obtained for the other layers. The layer's MI transfer characteristic is not affected by the *other* layers, and the cross-over point is determined only by the matching of the layer's equalizer and decoder EXIT curves given the channel realization and E_s/N_0.

Obviously, FER is a crucial requirement for AC schemes, for which the required FER's corresponding $I^{\mathrm{E(end)}}_{m,q}$ is one of the parameters for code selection. In this case, the scenario has to be avoided where the cross over between the two curves happens before $I^{\mathrm{D}}_{m,q} \approx 1$ is attained. As discussed with Fig. 4(b), such an event happens if the decoder feedback MI $I^{\mathrm{D}}_{m,q}$ obtained as a result of the first iteration is insufficient. For further convenience in notation, let $I^{\mathrm{D}}_{m,q}$ and $I^{\mathrm{E}}_{m,q}$ at the first iteration be denoted as $I^{\mathrm{D(start)}}_{m,q}$ and $I^{\mathrm{E(start)}}_{m,q}$, respectively. Note that $I^{\mathrm{E(start)}}_{m,q}$ is also independent of the other layers since the decoder feedback MI $I^{\mathrm{D}}_{m,q} = 0$ for all layers.

Now, we propose a simple scheme for AC, which is summarized as follows.

1) To achieve a high code rate, select a set $\mathcal{R}_{c1}$ of coding rates that satisfy $\gamma^{\alpha}_{\mathcal{R}} < I^{\mathrm{E(end)}}_{m,q}$, namely

$$\mathcal{R}_{c1} = \left\{ \mathcal{R} | \gamma^{\alpha}_{\mathcal{R}} < I^{\mathrm{E(end)}}_{m,q} \right\} \tag{37}$$

for each rate in the set of rates $\mathcal{R}$, where γ^{α}_{R} denotes the equalizer output MI required to yield FER $\leq \alpha$.

2) To avoid the cross over between the two curves before $I^{\mathrm{D}}_{m,q} \approx 1$ is attained, select a set $\mathcal{R}_{c2}$ of coding rates that satisfy $\gamma^{\beta}_{\mathcal{R}} < I^{\mathrm{E(start)}}_{m,q}$, namely

$$\mathcal{R}_{c2} = \left\{ \mathcal{R} | \gamma^{\beta}_{\mathcal{R}} < I^{\mathrm{E(start)}}_{m,q} \right\} \tag{38}$$

TABLE II
EXAMPLE OF PRECALCULATED TABLE

$\mathcal{R}$	1/8	1/7	1/6	1/5	1/4	1/3	1/2
$\gamma^{\alpha}_{\mathcal{R}}$	0.3183	0.3567	0.4040	0.4701	0.5545	0.6602	0.8197
$\gamma^{\beta}_{\mathcal{R}}$	0.0661	0.0778	0.0952	0.1169	0.1544	0.2276	0.3737
$\mathcal{R}$	2/3	3/4	4/5	5/6	6/7	7/8	
$\gamma^{\alpha}_{\mathcal{R}}$	0.9256	0.9509	0.9618	0.9714	0.9825	0.9848	
$\gamma^{\beta}_{\mathcal{R}}$	0.5345	0.6331	0.7000	0.7403	0.7716	0.7971	

for each rate in the set of rates $\mathcal{R}$, where $\gamma^{\beta}_{\mathcal{R}}$ denotes the equalizer output MI required to yield $I^{\mathrm{E(start)}} < G^{-1}_{\mathcal{R}}(\beta)$, which is equivalent to $I^{\mathrm{D(start)}} > \beta$. Thus, β denotes a threshold of the decoder feedback MI at the first iteration.

3) The allocated coding rate $R_{m,q}$ satisfies

$$R_{m,q} = \max\{\mathcal{R}_{c1} \cap \mathcal{R}_{c2}\}. \tag{39}$$

4) If $\mathcal{R}_{c1} \cap \mathcal{R}_{c2}$ is null, then

$$R_{m,q} = [\text{the lowest rate in the available code set}].$$

In the AC scheme described above, the system design parameters α and β have to be chosen so that the FER requirements can be satisfied.[3] Furthermore, the values of $\gamma^{\alpha}_{\mathcal{R}}$ and $\gamma^{\beta}_{\mathcal{R}}$ have to be precalculated for each code in the code set. An example of the precalculated $\gamma^{\alpha}_{\mathcal{R}}$ and $\gamma^{\beta}_{\mathcal{R}}$ values is summarized for the convolutional codes listed in Table II for $\alpha = 0.1$ and $\beta = 0.15$. The $\gamma^{\alpha}_{\mathcal{R}}$ that satisfies the FER requirement, which is represented by α, can easily be determined by using Fig. 3(b), where it

[3]The proposed technique is, in fact, empirical, for which the selected code is suboptimal. Such suboptimality is due to the practicality reason of avoiding the necessity for the online calculation of multidimensional EXIT functions.

is found that the relationship between FER and the required equalizer output MI is one to one. The major aim of setting the parameter $\gamma_{\mathcal{R}}^{\beta}$ is to avoid the intersection between the EXIT curves and to enhance the total throughput, the details of which are provided in Section IV. Note that Fig. 4(a) and (b) is for the cases of $\beta = 0.8$ and $\beta = 0$, respectively, for both of which $\alpha = 0.1$. The influence of the choice of the β value is investigated in Section IV through simulations.

C. Empirical Method for MI Calculation

To exactly calculate the MI, perfect knowledge about the transmitted bit sequence is needed when evaluating the pdf $p_{\lambda|c}(\xi|\mathcal{C})$ of the likelihood. However, in practice, MI has to be calculated without knowing the transmitted coded sequence at the Rx side.

Applying Bayes' theorem $p_{\lambda|c}(\xi|\mathcal{C}) = 2p_{\lambda}(\xi)p_{c|\lambda}(\mathcal{C}|\xi)$ to (32), the MI is rewritten as

$$\begin{aligned}\mathcal{I} &= 1 - 2\int_{-\infty}^{\infty} p_{\lambda}(\xi)p_{c|\lambda}(+1|\xi)\log_2(1+e^{-\xi})d\xi \\ &= 1 - 2\mathbb{E}\left\{p_{c|\lambda}(+1|\xi)\log_2(1+e^{-\xi})\right\} \end{aligned} \tag{40}$$

where $p_{\lambda}(\xi)$ is obtained through the LLR histogram measurement. Applying Bayes' theorem, $p_{c|\lambda}(+1|\xi)$ is given by

$$\begin{aligned} p_{c|\lambda}(+1|\xi) &= e^{\xi}p_{c|\lambda}(-1|\xi) = e^{\xi}\left[1 - p_{c|\lambda}(+1|\xi)\right] \\ &= \left[1+e^{-\xi}\right]^{-1} \end{aligned} \tag{41}$$

where the consistency condition of (33) has been used. By invoking the ergodicity, the expectation can be replaced by the time average as

$$\mathcal{I} = 1 - \frac{1}{K}\sum_{k'=1}^{2K}\frac{\log_2\left(1+\exp\left(-\lambda\left[c(k')\right]\right)\right)}{1+\exp\left(-\lambda\left[c(k')\right]\right)} \tag{42}$$

where $\lambda[c(k')]$ is the LLR of the k'th-coded bit in the frame LLR having length of $2K$. Note that this empirical method may deteriorate the MI accuracy due to the approximations used in LLR calculation, as in the Max Log-Map algorithm in which the consistency condition may not necessarily be perfectly satisfied. It is now obvious that an MI trajectory online measurement can be easily performed by using (42), along with the turbo iterations.

IV. Channel-Model-Based Simulation

The results of a series of simulations conducted to verify the throughput enhancement achieved by the proposed AC technique are presented in this section. Spatially uncorrelated two Tx and two Rx antennas were assumed $(M = N = 2)$. For each of the Tx–Rx antenna pairs, a 24-path $(L = 24)$ Rayleigh-fading channel with an average path energy having a decaying factor of 2 dB between consecutive paths was assumed. Perfect knowledge about the channels was assumed available at the Rx. The Max Log-MAP algorithm with a correcting factor proposed in [23] was used in each layer's SISO decoder. The turbo Rx performed eight iterations of the equalization and decoding chain. The transmitted signal was a multilevel-coded 16-QAM symbol sequence with symbol rate of $S_r = 20$ Msymbols/s. $K = 2048$ and $P = 64$ were assumed. Table III summarizes the major simulation specifications.

TABLE III
Parameters of Model-Based Simulation

Modulation	16QAM $(Q = 4)$
Symbol rate S_r	20 Msymbols/sec
Data Symbol length K	2048 symbols
Cyclic prefix length P	64 symbols
Coded bits length $2K$	4096 bits
Channel coding	non-systematic convolutional code (constraint length 4)
Decoder	Max-Log-MAP with correction factor
Interleaver	Random
iteration	8
Number of antennas	Tx:2 , Rx:2
Channel model Delay profile	24-path Rayleigh fading exponentially 2 dB decaying
Channel estimation	Perfect

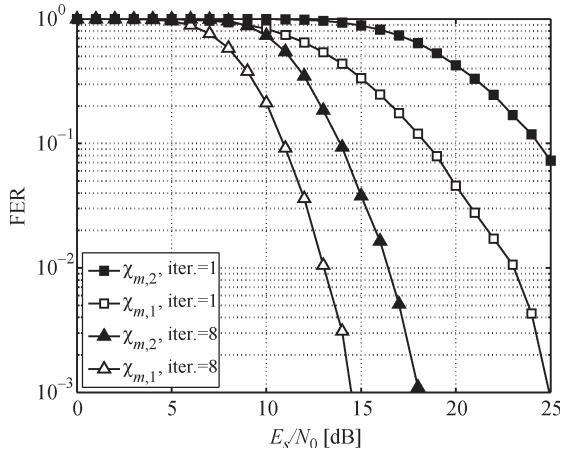

Fig. 5. FER versus the average E_s/N_0 per receive antenna at the first and eighth iterations. The code rate is 0.5 for all layers.

When evaluating the throughput efficiency, an ideal selective-repeat ARQ [7] was assumed. The instantaneous throughput is only associated with the frame being transmitted. The layer $\chi[m,q]$'s supported throughput $\eta_{m,q}$ and the overall throughput η totaling over the all layers are, respectively, defined as $\eta_{m,q} = S_r D_{m,q}/(P+K)$ and $\eta = \sum_{m=1}^{M}\sum_{q=1}^{Q/2}\eta_{m,q}$, where $D_{m,q}$ denotes the number of information bits in a frame received without errors. Obviously, if the frame is received in error, $D_{m,q} = 0$; otherwise, $D_{m,q} = 2KR_{m,q}$. The average throughput is defined by the ratio of the total number of information bits received without error to the total number of transmitted bits, where fading variations on the path components were assumed to be statistically independent at each frame transmission. In the simulations, 50 000 frames were transmitted for each average E_s/N_0 per receive antenna value evaluated.

Figs. 5 and 6 show the results of the simulation for FER and throughput efficiency versus the average E_s/N_0, respectively, with the fixed code rate ML-BICM, where the code rate $R_{m,q}$ was fixed to be half for all the layers. Note that the curves shown

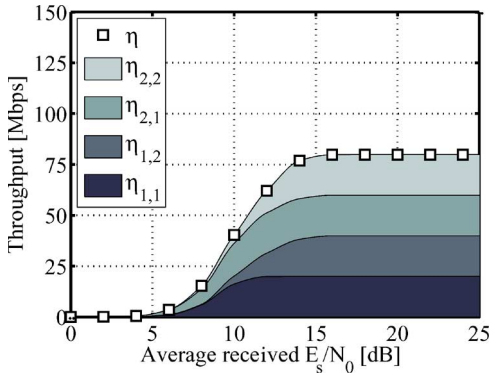

Fig. 6. Average throughput versus E_s/N_0 per receive antenna protect property with selective-repeat ARQ. The code rate is 0.5 for all layers.

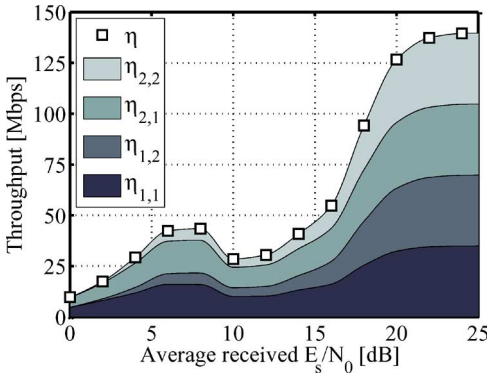

Fig. 7. Average throughput versus E_s/N_0 per receive antenna property with AC ($\alpha = 0.1$, and $\beta = 0$).

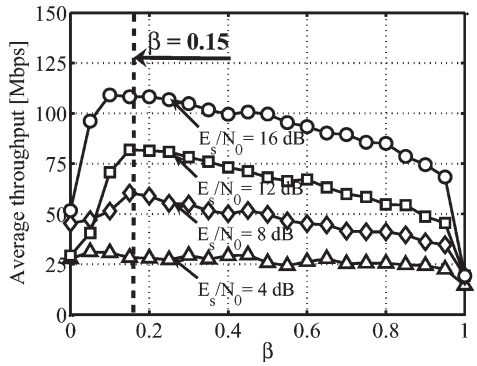

Fig. 8. Average throughput versus the β threshold property for the proposed AC scheme.

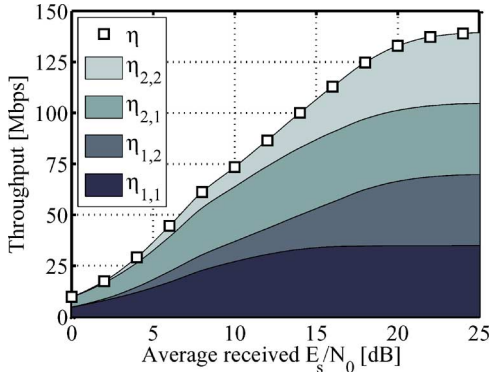

Fig. 9. Average throughput versus E_s/N_0 per receive antenna property with AC ($\alpha = 0.1$, and $\beta = 0.15$).

in Fig. 6 indicate the *cumulative* throughput efficiencies that sum up the transmitted bits, which are correctly received, in the increasing order of the layers. It is found from Fig. 5 that the FER curves are separated according to the layers.

Fig. 7 shows the throughput efficiency of the proposed ML-BICM AC scheme with $\beta = 0$; therefore, the code rates are only determined by the FER requirement of $\alpha = 0.1$. It is found from the figure that there are small "*humps*" in all the $\eta_{m,q}$ curves around $E_s/N_0 = 10$ dB. This is because with $\beta = 0$, the equalizer and decoder MI curves cross with a recognizable probability before the target MI is achieved. Fig. 8 shows for $M = 2$, $N = 2$, and $Q = 4$ that the average throughput performance versus the β value with the average E_s/N_0 as a parameter. It is found from the figure that the average throughput is maximized with $\beta = 0.15$. With $\beta = 0.15$, the average throughput performance of the proposed AC scheme versus the average E_s/N_0 is shown in Fig. 9. By making a comparison between Figs. 6 and 9, it is found that the proposed AC scheme can significantly improve the throughput performance over the fixed code rate ARQ. Without AC, the layers $\chi[1, 2]$ and $\chi[2, 2]$ do not make any significant contribution to the total throughput when the average $E_s/N_0 \leq 10$ dB. This is because the code rate is fixed for any channel realization. In contrast, the proposed AC scheme allows the layers to adaptively adjust the code rates given channel realizations, by which they all make contributions to the total throughput. When the average E_s/N_0 is large enough, the total throughput plateaus at the sum of the code rates allocated for both schemes. However, the AC achieves a much higher throughput because higher than half code rates can be used, whereas it is fixed without AC. Therefore, if a higher-order modulation is used, the maximum throughput will further increase with AC.

V. Measurement-Data-Based Assessment

The performances of MIMO systems deeply depend on the spatial–temporal multipath structure at both Tx and Rx sides. In the previous section, we assumed a scattering-rich environment to verify the maximum throughput. In fact, the scattering richness provides a higher MIMO capacity [24], [25]. However, in realistic scenarios, the channel's spatial properties vary depending on the surrounding terrain's geographical structure, which results in the variation in the rank of the correlation matrix constructed from the channel matrix: The extreme cases are the line-of-sight (LOS) and fully multipath-rich scenarios. Since ML-BICM AC adaptively adjusts the code parameters with the aim of throughput enhancement given channel realizations, the effectiveness of the proposed scheme has to be verified in realistic conditions for practical considerations.

To assess the practicality of the proposed ML-BICM AC scheme in real fields, a series of simulations using multidimensional channel-sounding field measurement was conducted. An advantageous point of the channel-sounding field-measurement-data-based simulation is that the performance results can be correlated with the channel's spatio and temporal characteristics analyzed by using the same data set. It

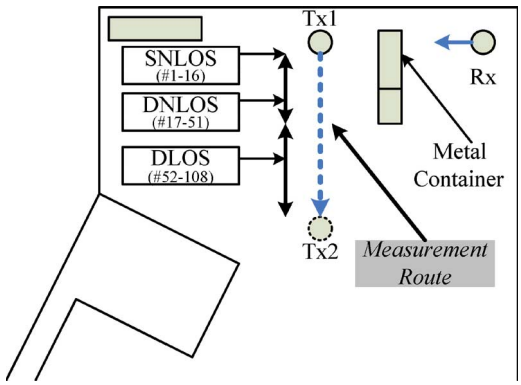

Fig. 10. Field map of measurement field.

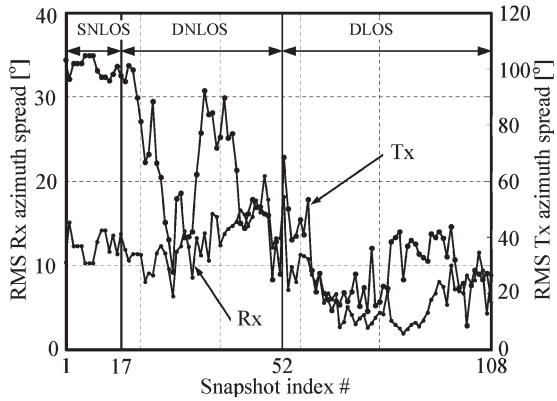

Fig. 11. Azimuth spread properties at both Tx and Rx.

TABLE IV
PARAMETERS OF THE MEASUREMENT CAMPAIGN

Measurement frequency	5.2 GHz
Transmitter	UCA, 16 antennas, spacing of 0.5λ
Receiver	ULA, 8 antennas, spacing of 0.4λ
Transmitter height	2.1 m
Receiver height	1.62 m
Measurement bandwidth	120 MHz
Transmit and receive filter	root Nyquist raised cosine, roll off factor 0.25
Data rate	20 MHz
Required band width	25 MHz
Number of multipath components after receive filtering	L = 24

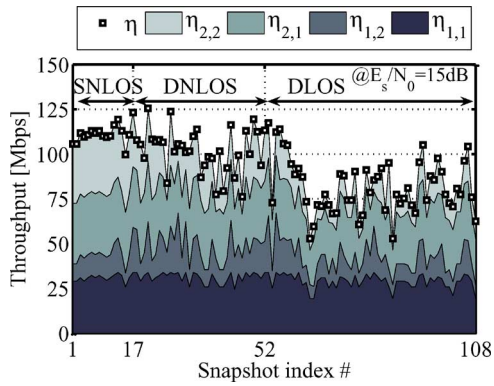

Fig. 12. Throughput performance in the case where the instantaneous protect received signal power is kept constant.

is made possible to trace back the observed algorithm behavior, and by correlating the obtained performance tendency with the channel analysis results, we can know how the algorithm has behaved in real fields.

A bidirectional multidimensional channel-sounding measurement campaign took place in a large courtyard at the campus of Ilmenau University of Technology, Ilmenau, Germany, which is shown in Fig. 10. A 16-element uniform circular array (UCA) with minimum element spacing of half the wavelength was used as the Tx antenna, and the Tx was moved at a walking speed along the route marked by the dashed line in the figure. Further, an eight-element uniform linear array (ULA) with element spacing of 0.4 wavelength was used as the Rx antenna, and the Rx position was fixed. The area was surrounded by buildings with a height of approximately 15 m, and there was a metal object on the front-side angle of the Rx array. The first 3 m of the measurement route is behind the metal object; therefore, this region is characterized as a non-LOS (NLOS) part. Table IV summarizes the major specifications of the measurement campaign.

Fig. 11 shows the root-mean-squared azimuth spreads at both Tx and Rx sides, which were obtained by using the RIMAX framework [7], [13], versus the snapshot number. The total number of snapshots gathered along the measurement route is 108. Looking at Fig. 11, it is found that snapshot #52 is a border point between NLOS and LOS. In addition, since Tx was fixed between snapshots #1 and #16, they are referred to as static NLOS (SNLOS). In the rest of the snapshots, Tx moved along the route. Therefore, snapshots #17–#51 and #52–#108 are refereed to as dynamic NLOS (DNLOS) and dynamic LOS (DLOS), respectively. The two elements were selected from the array antenna elements at both Tx and Rx sides, which result in 2×2 MIMO channels. Two antenna elements having the largest spacing, which are located on the diameter of the UCA and on both ends of the ULA, at the Tx and Rx, respectively, were used. The spacings of the two antenna elements used were 2.56 and 2.8 times the wavelength, respectively, at the Tx and Rx.

Fig. 12 shows the throughput efficiencies supported by the four layers of the proposed ML-BICM AC versus the snapshot number. Power control was performed so that the *instantaneous* E_s/N_0 sets at 15 dB. The figure clearly shows that the variation in azimuth spread is a dominating factor for throughput efficiency when the instantaneous E_s/N_0 is fixed. It is found that in LOS environments, the throughput can only reach approximately 80 Mb/s, although 105 Mb/s is achieved in the NLOS environment. This is because the less is the scattering-rich environment, the lower is the azimuth spreads in LOS environments, as shown in Fig. 11, which results in the lower channel capacity of MIMO systems.

Fig. 13 shows the MIMO channel capacity for the channel realization given by the measurement data and the total throughput achieved by the proposed ML-BICM AC versus the

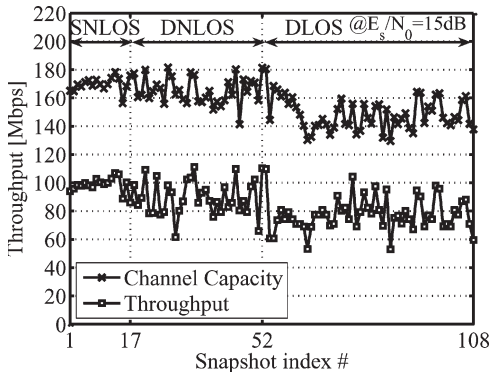

Fig. 13. Comparison between ML-BICM AC and channel capacity.

snapshot number. The channel capacity in frequency-selective MIMO channels is given by

$$C_{\mathrm{MIMO}} = \frac{W}{K}\sum_{k=1}^{K}\log_2\det\left[\boldsymbol{I} + \frac{E_s K}{N_0 M}\boldsymbol{\Xi}(k)\boldsymbol{\Xi}^H(k)\right] \quad (43)$$

where W is the bandwidth corresponding to S_r, and $\Xi(k)$ is the frequency-domain channel response observed at the kth frequency bin, the details of which are given in the Appendix. It is found that the variations of the channel capacity and the throughput achieved by ML-BICM AC are highly correlated. The correlation confirms the proposed AC scheme's potential of well exploiting the channel's information-bearing capability. However, there is still a gap between the channel capacity and the throughput achieved by the proposed ML-BICM AC scheme. The use of stronger and more flexible codes should reduce the gap between the two curves.

VI. Summary

An efficient AC scheme for ML-BICM with MMSE turbo equalization has been proposed in this paper. The primary purpose of the proposed scheme is to minimize the information rate loss due to the mismatch between channel realization and channel coding. The proposed scheme allows for efficient MIMO turbo equalization at the Rx to be performed and provides a high data throughput and its robustness in varying spatiotemporal channel characteristics. This is a major outcome of adaptive code parameter selection based on the knowledge of EXIT characteristics at the Rx. Numerical performance results showed that the throughput efficiency can be significantly improved with the proposed AC scheme over the ARQ with fixed coding rate. Furthermore, the effectiveness of the proposed scheme in real fields was demonstrated through a series of field-measurement-data-based simulations.

Appendix
Frequency-Domain MMSE Equalization

To determine the optimum tap coefficients in MMSE filtering without requiring high computational complexity, a frequency-domain processing technique described in [17] is used with minor modifications to fit with the ML-BICM signaling. By applying the matrix inversion lemma to (27), the filter output can be expressed as

$$\boldsymbol{z}_m = (1+\overline{\gamma}_m\overline{\delta}_m)^{-1}[\overline{\gamma}_m\hat{\boldsymbol{s}}_m + \boldsymbol{F}^H\boldsymbol{\Psi}_m\boldsymbol{F}_N\tilde{r}] \quad (44)$$

where

$$\boldsymbol{\Psi}_m = \boldsymbol{\Xi}_m^H\left(\boldsymbol{\Xi}\boldsymbol{\Delta}\boldsymbol{\Xi}^H + \sigma_\nu^2\boldsymbol{I}_{NK}\right)^{-1} \quad (45)$$

$$\overline{\gamma}_m = \frac{1}{K}\mathrm{trace}[\boldsymbol{\Psi}\boldsymbol{\Xi}_m] \quad (46)$$

with

$$\Delta = \left(\boldsymbol{I}_{MK} - \mathrm{diag}\left[\overline{\boldsymbol{\delta}}\right]\right)\otimes\boldsymbol{I}_K \quad (47)$$

$$\overline{\boldsymbol{\delta}} = [\overline{\delta}_1,\ldots,\overline{\delta}_m,\ldots,\overline{\delta}_M] \quad (48)$$

$$\overline{\delta}_m = \frac{1}{K}\sum_{k=1}^{K}|\hat{s}_m(k)|^2\,. \quad (49)$$

Note that $\otimes$ and $\boldsymbol{I}_x$ denote the Kronecker product and an $x\times x$ square identity matrix, respectively.[4]

The frequency-domain channel response Ξ of $\boldsymbol{H}$ is then defined by

$$\begin{aligned}\boldsymbol{\Xi} &= \boldsymbol{F}_N\boldsymbol{H}\boldsymbol{F}_M^H \\ &= [\boldsymbol{\Xi}_1,\ldots,\boldsymbol{\Xi}_m,\ldots,\boldsymbol{\Xi}_M] \quad (50)\\ \boldsymbol{\Xi}_m &= [\boldsymbol{\Xi}_{1,m},\ldots,\boldsymbol{\Xi}_{n,m},\ldots,\boldsymbol{\Xi}_{N,m}]^T \quad (51)\\ \boldsymbol{\Xi}_{n,m} &= \boldsymbol{F}\boldsymbol{H}_{n,m}\boldsymbol{F}^H \quad (52)\end{aligned}$$

where $\boldsymbol{F}$ is a $K\times K$ discrete Fourier transform matrix operator with elements

$$[\boldsymbol{F}]_{x,y} = K^{\frac{1}{2}}e^{-i\frac{2\pi}{K}}(x-1)(y-1) \quad (53)$$

and $\boldsymbol{F}_x = \boldsymbol{I}_x\otimes\boldsymbol{F}$. Note that $\Xi_{n,m}$ is a diagonal matrix since $\boldsymbol{H}_{n,m}$ is a circular matrix. Now, we focus only on diagonal elements and define the following frequency-domain channel response observed at the kth frequency bin as

$$\boldsymbol{\Xi}(k) = [\boldsymbol{\Xi}_1(k),\ldots,\boldsymbol{\Xi}_m(k),\ldots,\boldsymbol{\Xi}_M(k)] \quad (54)$$

$$\boldsymbol{\Xi}_m(k) = [\Xi_{1,m}(k),\ldots,\Xi_{n,m}(k),\ldots,\Xi_{N,m}(k)] \quad (55)$$

$$\mathrm{diag}[\boldsymbol{\Xi}_{n,m}] = [\Xi_{n,m}(1),\ldots,\Xi_{n,m}(k),\ldots,\Xi_{n,m}(K)] \quad (56)$$

where diag[·] denotes a matrix operator that extracts only diagonal elements in the matrix. Note that $\Xi(k)$ was used in (43) when calculating the capacity of the frequency-selective MIMO channel. The first and second moments denoted as μ_m and σ_m^2 in the Gaussian approximation of (29) are, respectively, calculated by

$$\begin{aligned}\mu_m &= \mathrm{E}\left\{z_m(k)\right\} = \overline{\gamma}_m(1+\overline{\gamma}_m\overline{\delta}_m)^{-1} \quad (57)\\ \sigma_m^2 &= \mathrm{E}\left\{|z_m(k)|^2\right\} - \mu_m^2 \\ &= (1+\overline{\gamma}_m\overline{\delta}_m)^{-2}\left(\overline{\gamma}_m^2\overline{\delta}_m + \overline{\gamma}_m\right) - \mu_m^2 \\ &= \mu_m - \mu_m^2. \quad (58)\end{aligned}$$

[4] $\boldsymbol{I}_{MK}$ in (47) is attributed to $1/K\sum_{k=1}^{K}\mathbb{E}\{|s_m(k)|^2\}$. Since the average energy of symbol constellations is normalized to 1, the term reduces to an identity matrix in the case where frequency-domain turbo equalization with QAM signaling is employed.

ACKNOWLEDGMENT

The authors would like to thank MEDAV GmbH for providing the field measurement data obtained by using the RUSK MIMO channel sounder, the colleagues at the Centre for Wireless Communications, University of Oulu, for their comments and suggestions, and the colleagues at Ilmenau University of Technology for conducting the measurements and data analysis.

REFERENCES

[1] C. Douillard, M. Jezequel, C. Berrou, A. Picart, P. Didier, and A. Glavieux, "Iterative correction of intersymbol interference: Turbo-equalization," *Eur. Trans. Telecommun.*, vol. 6, no. 5, pp. 507–511, Sep. 1995.

[2] X. Wang and H. V. Poor, "Iterative (turbo) soft interference cancellation and decoding for coded CDMA," *IEEE Trans. Commun.*, vol. 47, no. 7, pp. 1046–1061, Jul. 1999.

[3] M. Tüchler and J. Hagenauer, "Turbo equalization using frequency domain equalizers," in *Proc. Allerton Conf.*, Monticello, IL, Oct. 2000, pp. 1234–1243.

[4] D. Reynolds and X. Wang, "Low complexity turbo-equalization for diversity channels," *Signal Process.*, vol. 81, no. 5, pp. 989–995, May 2001.

[5] A. Dejonghe and L. Vandendorpe, "Bit-interleaved turbo equalization over static frequency selective channels: Constellation mapping impact," *IEEE Trans. Commun.*, vol. 52, no. 12, pp. 2061–2065, Dec. 2004.

[6] G. Caire, G. Taricco, and E. Biglieri, "Bit-interleaved coded modulation," *IEEE Trans. Inf. Theory*, vol. 44, no. 3, pp. 927–946, May 1998.

[7] K. Kansanen, C. Schneider, T. Matsumoto, and R. Thomä, "Multilevel coded QAM with MIMO turbo-equalization in broadband single-carrier signaling," *IEEE Trans. Veh. Technol.*, vol. 54, no. 3, pp. 954–966, May 2005.

[8] S. Ibi, T. Matsumoto, S. Sampei, and N. Morinaga, "EXIT chart-aided adaptive coding for MMSE turbo equalization with multilevel BICM," *IEEE Commun. Lett.*, vol. 10, no. 6, pp. 486–488, Jun. 2006.

[9] T. Abe and T. Matsumoto, "Space–time turbo equalization in frequency-selective MIMO channels," *IEEE Trans. Veh. Technol.*, vol. 52, no. 3, pp. 469–475, May 2003.

[10] C. Schneider, R. Thomä, U. Trautwein, and T. Matsumoto, "The dependency of turbo MIMO equalizer performance on the spatial and temporal multipath channel structure—A measurement based evaluation," in *Proc. VTC*, Jeju, Korea, Apr. 22–25, 2003, vol. 2, pp. 808–812.

[11] S. ten Brink, "Convergence behavior of iteratively decoded parallel concatenated codes," *IEEE Trans. Commun.*, vol. 49, no. 10, pp. 1727–1737, Oct. 2001.

[12] R. Thomä, D. Hampicke, A. Richter, G. Sommerkorn, A. Schneider, U. Trautwein, and W. Wirnitzer, "Identification of time-variant directional mobile radio channels," *IEEE Trans. Instrum. Meas.*, vol. 49, no. 2, pp. 357–364, Apr. 2000.

[13] R. Thomä, M. Landmann, and A. Richter, "RIMAX—A maximum likelihood framework for parameter estimation in multidimensional channel sounding," in *Proc. Int. Symp. Antennas Propag.*, Sendai, Japan, Aug. 2004, pp. 53–56.

[14] R. Thomä, M. Landmann, A. Richter, and U. Trautwein, "Multidimensional high-resolution channel sounding," in *Smart Antennas in Europe-State-of-the-Art*, vol. 3, T. Kaiser *et al.*, Eds. New York: Hindawi, 2005.

[15] U. Trautwein, C. Schneider, and R. Thomä, "Measurement-based performance evaluation of advanced MIMO transceiver designs," *EURASIP J. Appl. Signal Process.*, vol. 2005, no. 11, pp. 1712–1724, 2005.

[16] M. S. Yee, M. Sandell, and Y. Sun, "Comparison study of single-carrier and multi-carrier modulation using iterative based receiver for MIMO system," in *Proc. VTC—Spring*, Milan, Italy, May 2004, vol. 3, pp. 1275–1279.

[17] K. Kansanen, "Wireless broadband single-carrier systems with MMSE turbo equalization receivers," Ph.D. dissertation, Univ. Oulu, Oulu, Finland, Dec. 2005.

[18] G. Bauch and V. Franz, "A comparison of soft-in/soft-out algorithms for turbo detection," in *Proc. Int. Conf. Telecommun.*, Porto Carras, Greece, Jun. 1998, pp. 259–263.

[19] S. ten Brink, J. Speidel, and R.-H. Yan, "Iterative demapping and decoding for multilevel modulation," in *Proc. GLOBECOM*, Sydney, Australia, Nov. 1998, pp. 579–584.

[20] P. Magniez, B. Muquet, P. Duhamel, and M. de Courville, "Improved turbo-equalization with application to bit-interleaved modulations," in *Proc. Asilomar Conf. Signals, Syst., Comput.*, Pacific Grove, CA, Oct. 2000, vol. 2, pp. 1786–1790.

[21] J. Hagenauer, "The EXIT chart—Introduction to extrinsic information transfer in iterative processing," in *Proc. 12th EUSIPCO*, Sep. 2004, pp. 1541–1548.

[22] J. G. Proakis, *Digital Communications*, 4th ed. New York: McGraw-Hill, 2001.

[23] P. Robertson, E. Villebrun, and P. Hoeher, "A comparison of optimal and sub-optimal MAP decoding algorithms operating in the log domain," in *Proc. ICC*, Seattle, WA, Jun. 1995, pp. 1009–1013.

[24] G. J. Foschini and M. J. Gans, "On limits of wireless communications in a fading environment when using multiple antennas," *Wirel. Pers. Commun.*, vol. 6, no. 3, pp. 311–335, Mar. 1998.

[25] I. E. Telatar, "Capacity of multi-antenna Gaussian channels," *Eur. Trans. Telecommun.*, vol. 10, no. 6, pp. 585–596, Nov. 1999.

Shinsuke Ibi (S'02–M'07) was born in Nagoya, Japan, in 1978. He received the B.E. degree in advanced engineering from Suzuka College of Technology, Suzuka, Japan, in 2002 and the M.E. and Ph.D. degrees from Osaka University, Osaka, Japan, in 2004 and 2006, respectively.

From 2005 to 2006, he was a Visiting Researcher with the Centre for Wireless Communications, University of Oulu, Oulu, Finland. Since 2007, he has been with the Faculty of Engineering, Osaka University, where he is currently an Assistant Professor with the Department of Information and Communications Technology. His research interests include EXIT-based coding theory, iterative decoding, multiuser detection, and communication theory.

Dr. Ibi was the recipient of the 3rd YRP Encouragement Award, the IEEE Vehicular Technology Society Japan 2003 Young Researcher's Encouragement Award, and the Institute of Electrical, Information, and Communication Engineers 2004 Active Research Award in Radio Communication Systems.

Tad Matsumoto (M'84–SM'95) received the B.S., M.S., and Ph.D. degrees from Keio University, Yokohama, Japan, in 1978, 1980, and 1991, respectively, all in electrical engineering.

In April 1980, he was with Nippon Telegraph and Telephone Corporation (NTT), Tokyo, Japan, where he was involved in many research and development projects, all for mobile wireless communications systems. In July 1992, he was with NTT DoCoMo, Tokyo, where he researched code-division multiple-access techniques for mobile communication systems. From 1992 to 1994, he was a part-time Lecturer with Keio University, Tokyo. In April 1994, he was with NTT America, New York, NY, where he was a Senior Technical Advisor of a joint project between NTT and NEXTEL Communications. In March 1996, he returned to NTT DoCoMo, where he was the Head of the Radio Signal Processing Laboratory until August 2001, when he worked on adaptive signal processing, multiple-input–multiple-output turbo signal detection, interference cancellation, and space–time coding techniques for broadband mobile communications. Since May 2002, he has been with Oulu University, Oulu, Finland, where he is currently a Professor with the Centre for the Wireless Communications. He was a Visiting Professor with Ilmenau University of Technology, Ilmenau, Germany, funded by the German MERCATOR Visiting Professorship Program, until January 2007. Since April 2007, he has also been a Professor with the Japan Advanced Institute of Science and Technology, Ishikawa, Japan.

Dr. Matsumoto was a member of the Board of Governors of the IEEE Vehicular Technology Society from January 2002 to December 2004 and is serving again until December 2007. He received the IEEE Vehicular Technology Society Outstanding Service Award in 2001, the Nokia Foundation Visiting Fellow Scholarship Award in 2002, the IEEE Japan Council Award for Distinguished Service to the Society in 2006, the IEEE Vehicular Technology Society James R. Evans Avant Garde Award in 2006, and the Thuringen State Research Award for Advanced Applied Science in 2006. Recently, he has been re-elected as a board member of the society from January 2008 to December 2010. He has been appointed a Finnish Distinguished Professor from January 2008 to December 2012, funded by the Finnish National Technology Agency (Tekes) and Finnish Academy.

Reiner Thomä (M'92–SM'00–F'07) received the Dipl.-Ing., Dr.-Ing., and Dr.-Ing. habil. degrees from Ilmenau University of Technology, Ilmenau, Germany, in 1975, 1983, and 1989, respectively, all in electrical engineering (information technology).

Since 1992, he has been a Professor of electrical engineering (electronic measurement engineering) with Ilmenau University of Technology. He is involved in various German and European research clusters, the European network of excellence NEWCOM, and is the speaker for the German national research program "Ultrawide-Band Radio Technologies for Communication, Localization, and Sensor Technology." His research interests include digital signal analysis, sensor array signal processing, parameter estimation, and system identification methods and their application in mobile radio propagation measurement and UWB sensor systems. This includes multidimensional propagation parameter estimation techniques, source localization, and position tracking.

Dr. Thomä is a member of Verband Deutscher Ingenieure/ Informationstechnische Gesellschaft and the International Scientific Radio Union (Comm. A). He is the Chairman of the IEEE Instrumentation and Measurement Society Technical Committee TC-13 "Wireless and Telecommunications."

Seiichi Sampei (M'88–SM'01–F'07) was born in Yokohama, Japan, in 1957. He received the B.E., M.E., and Ph.D. degrees from Tokyo Institute of Technology, Tokyo, Japan, in 1980, 1982, and 1991, respectively, all in electrical engineering.

From 1982 to 1993, he was a Researcher with the Communications Research Laboratory, Ministry of Posts and Telecommunications, Tokyo, where he was engaged in the development of adjacent channel interference rejection, fast-fading compensation, and M-ary QAM techniques for land-mobile communication systems. From 1991 to 1992, he was a Visiting Researcher with the University of California, Davis. Since 1993, he has been with the Faculty of Engineering, Osaka University, Osaka, Japan, where he is currently a Professor with the Department of Information and Communications Technology, and where he has developed adaptive modulation, intelligent radio transmission/access, and cognitive wireless networking techniques.

Dr. Sampei is a member of the Institute of Image Information and Television Engineers and a fellow of the Institute of Electrical, Information, and Communication Engineers (IEICE). He was the recipient of the Shinohara Young Engineering Award, the Achievements Award from the IEICE, the Telecom System Technology Award from the Telecommunication Advancement Foundation, and the DoCoMo Mobile Science Award from the Mobile Communication Fund.

Norihiko Morinaga (F'01) received the B.E. degree in electrical engineering from Shizuoka University, Shizuoka, Japan, in 1963, and the M.E. and Ph.D. degrees from Osaka University, Osaka, Japan, in 1965 and 1968, respectively.

In 1968, he was with the Department of Communications Engineering, Osaka University, where he was a Professor from 1987 to 2003 and worked in the area of radio, mobile, satellite, and optical communications systems, and EMC. He is a Professor Emeritus of Osaka University and currently a Professor with the Faculty of Engineering, Hiroshima International University, Hiroshima, Japan. He is currently promoting research on global intelligent wireless systems, which is achieved by a technological convergence of hardware and software, aiming to realize advanced information society.

Dr. Morinaga is a Fellow of the Institute of Electrical, Information and Communication Engineers (IEICE). He was the President of the Communication Society of the IEICE and the Vice President of the IEICE from May 1999 to May 2001. He was the General Chairman of the 10th International Symposium on Personal, Indoor and Mobile Radio Communications, Osaka, Japan, in 1999. He received the Telecom Natural Science Award and the Telecom System Technology Award from the Telecommunication Advancement Foundation, and the Paper Award, Achievements Award, and Distinguished Achievement and Contributions Award from the IEICE.